ORIGINAL ARTICLE

Application of Grey Relational Approach and Artificial Neural Network to Optimise Design Parameters of Bridge-Type Compliant Mechanism Flexure Hinge

Ngoc Thai Huynh[1] and Quoc Manh Nguyen[2,*]

[1]Faculty of Automotive Engineering Technology, Industrial University of Ho Chi Minh City, Ho Chi Minh City 700000, Vietnam
[2]Faculty of Mechanical Engineering, Hung Yen University of Technology and Education, Hung Yen, Vietnam

ABSTRACT – The investigation proposed a hybrid Grey-artificial neural network to optimise the design parameters of a two degree of freedom (2-DOF) bridge-type compliant mechanism flexure hinge (BTCMFH). The design variables play a vital role in determining the deformation and stress of the mechanism. The investigation is different from the previous studies where the hybrid method is a combination of grey relational analysis and artificial neural network based on finite element method (FEM) in ANSYS to maximise output displacement (DI) and minimise the stress (ST) of the mechanism. The simulation and ANOVA results identified the design variables have significantly affected the output displacement and stress by their contribution. The grey relational analysis and artificial neural network predicted values are in agreement with the simulation results at optimal combination parameters with a deviation error displacement and stress being 0.57% and 2.1%, respectively. The optimal combination parameters with a deviation error of displacement and stress of 0.52% and 2.1%, respectively. The optimal values of DI and ST were obtained as 0.957 mm and 104.74 MPa, respectively. The optimal value of displacement amplification ratio gained is 95.7.

INTRODUCTION

Classical joints always experience some form of clearance, causing oscillation and friction to occur, which induces wear in the joint. As a result, flexure hinge (FH) was designed, and it has since been applied in many mechanisms as a replacement for traditional joints. In this investigation, displacement amplification ratio (DAR) of 2-DOF BTCMFH was optimised by grey relational analysis (GRA) and artificial neural network (ANN).

In recent publications, many FHs with different shapes were investigated and fabricated to replace traditional joints. For instance, a circular FH was proposed for the kinetostatic modelling of 3-RRR compliant mechanisms by Yong and Lu [1]. The FHs were used as the rotation joints for a 3-DOF parallel mechanism for smooth and high precision motion in micro/nanomanipulation work, presented by Tian et al. [2]. A bridge-type compliant mechanism was designed by Qi et al. [3]. Qiu, Yin and Xie utilised the equivalent formula and the FEM to analyse failure in Triple-LET and LET flexure hinges [4]. Tian et al. used the finite element method to simulate flexible V-shaped hinges and compared them with the theory [5]. Yang et al. used super-elastic materials for a flexure hinge, and with their numerical computations and experiments were able to accurately forecast the displacement, along with effectively reducing the computation cost more than FEA by ANSYS [6]. Dao and Huang designed and optimised compliant mechanisms [7-12]. The Euler-Bernoulli beam theory was utilised to estimate the magnification ratio of compliant mechanisms by Xu and Li [13]. The effects of load on the magnification of compliant mechanisms were analysed and discussed by Liu and Yan [14]. Two FH compliant mechanisms were designed and fabricated by Ling et al. [15]. A bridge-type, fully compliant mechanism was proposed by Choi et al. [16], with outcomes confirmed by test and prior to publication. Ma et al. indicated that the magnification ratio has significantly influenced by the thickness of a flexure hinge [17]. Ling et al. [18] analysed and designed many kinds of FH.

In 2018, Ling et al. established a semi-analytical finite element model of complex compliant mechanisms using Lagrange's equation [19]. Sabri et al. performed an experiment to measure the displacement of silicon XY-microstages [20]. A new pseudo-rigid-body model of a flexure hinge was proposed by Šalinic et al. [21]. The principle of virtual work yielded a matrix relationship which was used to determine the quasi-static responses of a compliant mechanism due to external loads. Lai et al. used two L-shape lever-type mechanisms and one bridge-type mechanism to eliminate the bending moment and lateral forces [22]. The stiffness matrix method was applied to estimate the magnification ratio, and it was confirmed by FEM and experimentation. To meet essential needs such as large magnification, high rigidity, high-accuracy positioning and precision tracking, Wang and Zhang designed a compact planar three-degrees of freedom nano-positioning platform, in which, three two-level lever amplifiers were arranged symmetrically to obtain a larger magnification [23]. The kinematic and dynamic modelling precision was enhanced by the compensation afforded by the three displacement loss models and was determined by experimentation. The paper presents a design, and optimises the effects of design variables on DAR of a 2-DOF BTCMFH by using Grey relational analysis and artificial neural network based on the FEM in ANSYS software.

DESIGN MODEL AND ANALYSIS METHOD

The studied mechanisms have a total dimension of 70 mm length and 80 mm width and 10 mm thickness (see Figure 1). The design dimensions of the studied model are depicted in Figure 2. The design variables of the studied mechanism consist of input body length, the thickness of FH, incline angle between two FHs, and the width of FH.
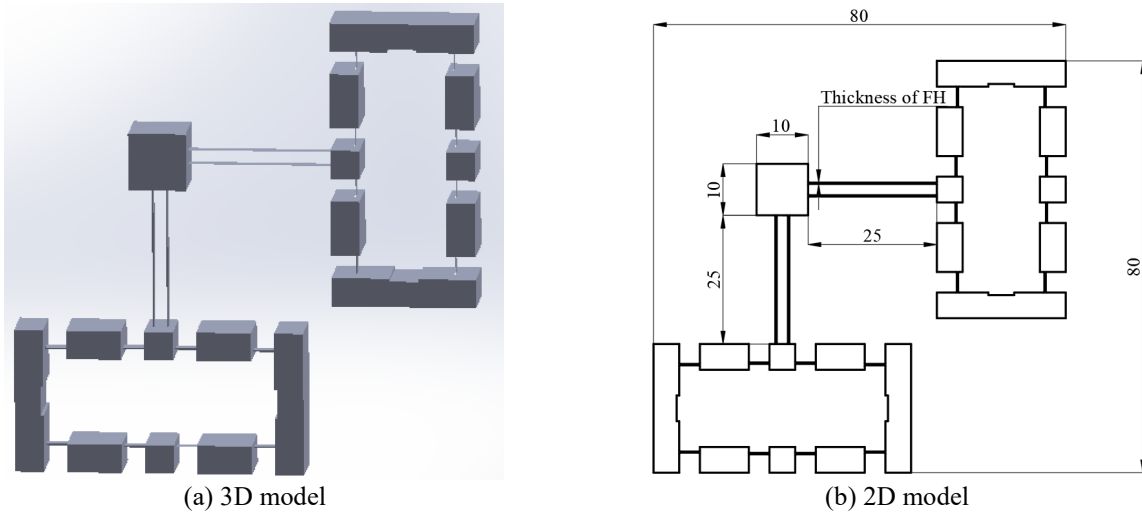

(a) 3D model   (b) 2D model

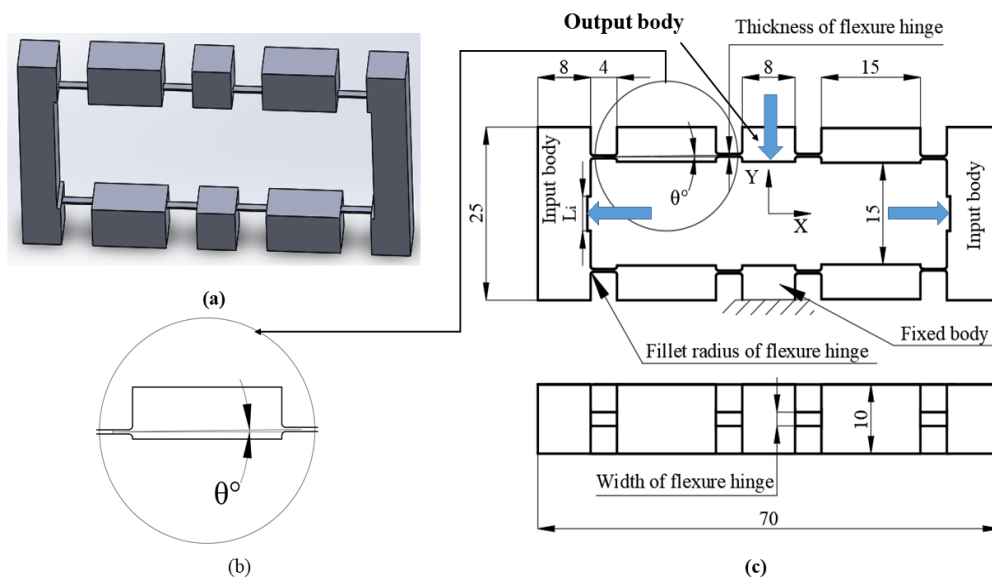**Figure 1.** 2-DOF of a bridge-type compliant mechanism flexure hinge.

Figure 2. Bridge-type compliant mechanism flexure hinge in (a) 3D, (b) 2D and (c) zoom in medium body and two FHs.

Table 1. Material mechanical properties.

Material	Young's modulus (GPa)	Poisson's ratio	Yield (MPa)
Aluminium	72	0.33	503

The model was designed by Solidworks and was inserted into a Static structural model of ANSYS. The AL-7075 aluminium was selected for the investigation with the parameters shown in Table 1. The mesh in the model was meshed by an automatic method. It is patch conforming in ANSYS, as illustrated in Figure 3(a) with 130524 nodes and 73352 kind of element is tetrahedron elements, respectively. The boundary conditions applied to the model are pointed out in Figure 3(b) with 0.01 displacement.
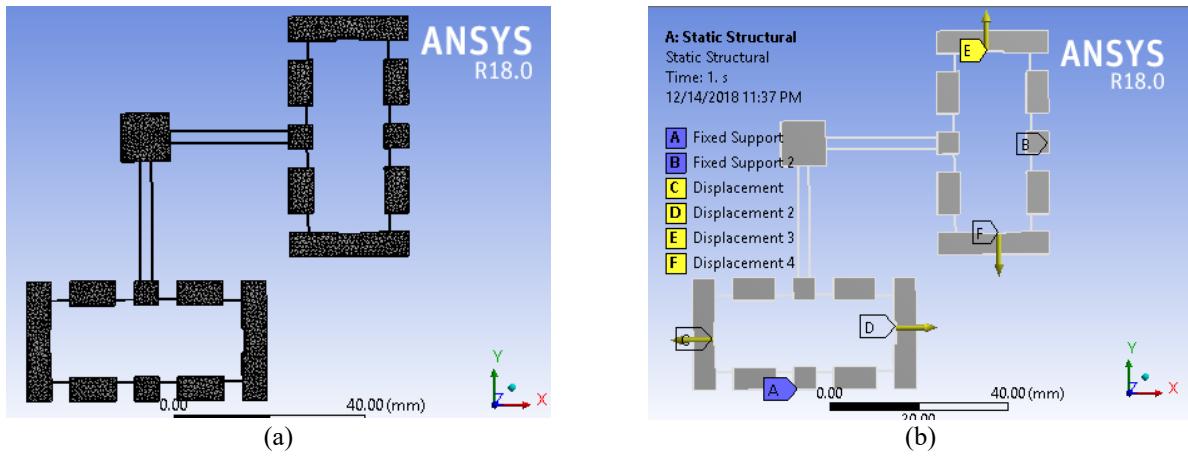
Figure 3. (a) The meshing model and (b) input boundary condition for the model.

OPTIMISATION METHODOLOGY

Grey Relational Analysis

Normalisation: Rewriting each sequence between 0 and 1 as follows [24-29]. The larger, the better for the mathematical formula:

$$D_i^* = \frac{D_i^{(0)}(k) - \min D_i^0(k)}{\max D_i^{(0)}(k) - \min D_i^{(0)}(k)} \tag{1}$$

The smaller, the better mathematical formula:

$$D_i^* = \frac{\max D_i^{(0)}(k) - D_i^0(k)}{\max D_i^{(0)}(k) - \min D_i^{(0)}(k)} \tag{2}$$

Grey relational coefficient (GRC) (γ) : A quantification method in the grey relational space. GRC is required before solving for the grey relational grade (GRG). The formula of deviation is calculated as follows:

$$\Delta_{0i} = \left\| D_0^*(k) - D_i^* k) \right\| \tag{3}$$

$$\Delta_{\min} = \max_{\forall j \in i} \min_{\forall k} \left\| D_0^*(k) - D_j^*(k) \right\| \tag{4}$$

$$\Delta_{\max} = \max_{\forall j \in i} \max_{\forall k} \left\| D_0^*(k) - D_j^*(k) \right\| \tag{5}$$

Calculating the grey relational coefficient (GRC),

$$\gamma_i(k) = \frac{\Delta_{\min} + \xi \Delta_{\max}}{\Delta_{0i} + \xi.\Delta_{\max}} \tag{6}$$

Here, $\xi \in [0,1]$ is the distinguishing coefficient, usually 0.5. By calculating the grey relational grade (GRG) and determine the weight,

$$\omega_e(x) = x.e^{(1-x)} + (1-x)e^x - 1 \tag{7}$$

where $\omega_e(x)$ is the mapping function in the entropy measurement. This function obtains the maximum value when $x = 0.5$ and $e^{0.5} - 1 = 0.6487$, and the mapping value in [0, 1] is obtained as follows:

$$w \equiv \frac{1}{(e^{0.5} - 1)} \sum_{i=1}^{m} \omega_e(x) \tag{8}$$

where $\in = \{\gamma_i(1), \gamma_i(2), ..., \gamma_i(n)\}$. Note that $i = 1, 2, ..., n$. Determining the total of the grey relational coefficient,

$$D_j \equiv \sum_{i=1}^{m} \gamma_i(j), j = 1, 2, ..., n \tag{9}$$

Estimating the normalised coefficient,

$$k = \frac{1}{(e^{0.5} - 1) \times m} = \frac{1}{0.6487 \times m} \tag{10}$$

Determining the entropy,

$$e_j = k \sum_{i=1}^{m} \omega_e(\frac{\gamma_i(j)}{D_j}), j = 1, 2, ..., n \tag{11}$$

Here, $\omega_e(x)$ uses Eq. (10). Computing the total of entropy:

$$E = \sum_{j=1}^{n} e_j \tag{12}$$

Determining the weight:

$$\omega_j = \frac{1}{n - E} \cdot \frac{[1 - e_j]}{\sum_{j=1}^{n} \frac{1}{n - E}[1 - e_j]}, here, j = 1, 2, ..., n \tag{13}$$

GRG (ψ_i) is the average value of GRC as follows:

$$\psi_i = \sum_{k=1}^{n} \omega_k \gamma_i(k) \tag{14}$$

Creating the table and response graph of GRG and analysing regression and analysis of variance of GRG. Predicting the output characteristics and GRG: output the acceleration, contact force and GRG can be estimated as:

$$\mu_D = D_m + \sum_{i=1}^{q} (D_0 - D_m) \tag{15}$$

$$\mu_\sigma = \sigma_m + \sum_{i=1}^{q} (\sigma_0 - \sigma_m) \tag{16}$$

$$\mu_G = G_m + \sum_{i=1}^{q} (G_0 - G_m) \tag{17}$$

where μ_D and μ_σ are the forecasted average values of the DI and ST, respectively; D_m and D_0 are the total of average values at the optimum level, and the average value of DI, respectively; σ_m and σ_0 are the total of average values at optimum level and the average value of ST; μ_G is the forecasted value of GRG; G_m is the average value of GRG at

optimum value; G_0 is the average value of GRG. The *(CI)* value was estimated at a 95% confidence level as in the following [30]:

$$CI_{CE} = \pm \sqrt{F_\alpha(1, fe)V_e\left(\frac{1}{n_{eff}} + \frac{1}{R_e}\right)} \tag{18}$$

Artificial Neural Network

This study used three layers, the input layer with five input parameters, the hidden layer with eleven neurons, and one output layer with one output neuron. The network is trained using the Levenberg-Marquardt hybrid (trainlm) [25, 31-33]. The structure of the artificial neural network is presented in Figure 3 and Figure 4. The input body length, incline angle, thickness, fillet radius and width of the FH were taken to be the input factors, and displacement or stress was taken as the output factors. The simulation values in Table 3 were utilised for training purposes. The simulation values in Tables 8 and 9 were utilised for testing purposes.
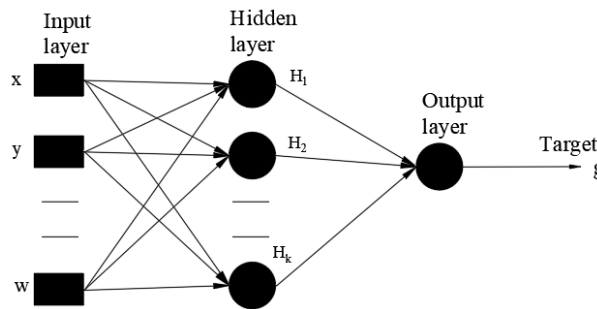

Figure 4. Structure of the ANN model in MATLAB with 5 input parameters, 11 neurons in the hidden layer and one output parameter.
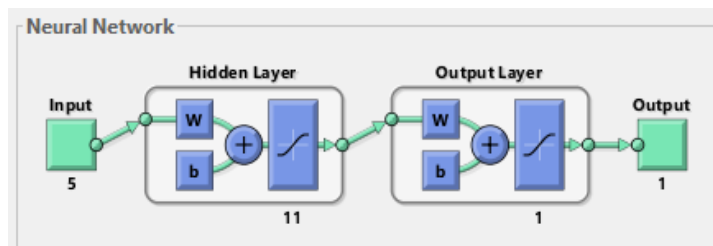

Figure 5. ANN training.

Statistical Analysis

The precision model is assessed by means of four error standards, as follows [34].
i.   The root mean squared error (RMSE) is the difference between forecast values and the simulation values or observed actual values:

$$RMSE = \sqrt{\frac{1}{m}\sum_{i=1}^{m}(x_i - y_i)^2} \tag{19}$$

ii.   The mean square error (MSE) is the square value of the root mean square:

$$MSE = \frac{1}{m}\sum_{i=1}^{m}(x_i - y_i)^2 \tag{20}$$

iii.   The mean absolute percentage error (MAPE):

$$MAPE = \frac{100\%}{m}\sum_{i=1}^{m}\left|\frac{x_i - y_i}{x_i}\right| \tag{21}$$

iv.   The coefficient of determination (R^2) must be at least 0.8 for forecast models to be accepted:

$$R^2 = 1 - \frac{\sum_{i=1}^{m}(x_i - y_i)^2}{\sum_{i=1}^{m}(x_i - \bar{y})^2} \quad (22)$$

where m is the number of simulation of experiments, x_i and y_i represent the simulation and predicting value, respectively, and $\bar{y}$ is the mean simulation value.

RESULTS AND DISCUSSION

Design Simulation

The design variables consist of five variables with three levels as presented in Table 2, which are: variable x changes of 5 mm, 10 mm and 15 mm, variable y changes of 0.25 mm, 0.5 mm and 0.75 mm, variable z changes of 0.8º, 1.2º, 1.6º, and WOFH changes of 2 mm, 4 mm and 6 mm. The orthogonal array and output deformation and stress, as listed in Table 3, were used to determine optimal values of DI and ST by Grey relational analysis and artificial neural network.

Table 2. Variables and values of variables.

Factor		Unit	Levels		
			1	2	3
Input body length	x	mm	5	10	15
TOFH	y	mm	0.25	0.5	0.75
Incline angle	z	degree	0.8	1.2	1.6
Fillet radius	t	mm	0.0	0.2	0.4
WOFH	w	mm	2	4	6

Table 3. Orthogonal arrays, displacement and stress.

Trial No.	x	y	z	t	w	Output displacement (mm)	Output stress (MPa)
1	5	0.25	0	0.8	2	0.90249	102.24
2	5	0.25	0.2	1.2	4	0.81073	98.789
3	5	0.25	0.4	1.6	6	0.70507	95.048
4	5	0.5	0	1.2	6	0.29433	80.808
5	5	0.5	0.2	1.6	2	0.41599	104.45
6	5	0.5	0.4	0.8	4	0.24688	80.995
7	5	0.75	0	1.6	4	0.18952	77.99
8	5	0.75	0.2	0.8	6	0.10081	89.578
9	5	0.75	0.4	1.2	2	0.18717	86.366
10	10	0.25	0	0.8	2	0.93349	100.77
11	10	0.25	0.2	1.2	4	0.84677	92.266
12	10	0.25	0.4	1.6	6	0.73869	90.243
13	10	0.5	0	1.2	6	0.34982	92.694
14	10	0.5	0.2	1.6	2	0.44157	111.12
15	10	0.5	0.4	0.8	4	0.28695	94.052
16	10	0.75	0	1.6	4	0.2236	93.235
17	10	0.75	0.2	0.8	6	0.12594	105.01
18	10	0.75	0.4	1.2	2	0.2095	98.191
19	15	0.25	0	0.8	2	0.95698	105.74
20	15	0.25	0.2	1.2	4	0.87465	95.132
21	15	0.25	0.4	1.6	6	0.76453	90.978
22	15	0.5	0	1.2	6	0.40407	106.8
23	15	0.5	0.2	1.6	2	0.46214	112.11
24	15	0.5	0.4	0.8	4	0.32527	110.48
25	15	0.75	0	1.6	4	0.25742	102.69
26	15	0.75	0.2	0.8	6	0.15518	93.71
27	15	0.75	0.4	1.2	2	0.22986	98.04

Influence of Variable *y*

The outcome of direction deformation (X-axis) and (Y-axis), as depicted in Figure 6, changed from 0.61 mm to 0.138 mm as variable y changes from 0.25 mm to 0.75 mm with input DI of 0.01 according to X-axis and Y-axis direction (with variable x of 5 mm, and variable z of 0.8º, variable w of 2 mm, and variable t of 0 mm). The analysis from FEM outcomes are larger than the references [1-4, 6]. The values of ST change from 120 MPa to 84.46 MPa, as seen in Figure 7. The result proved that two outputs had significantly influenced variable y.
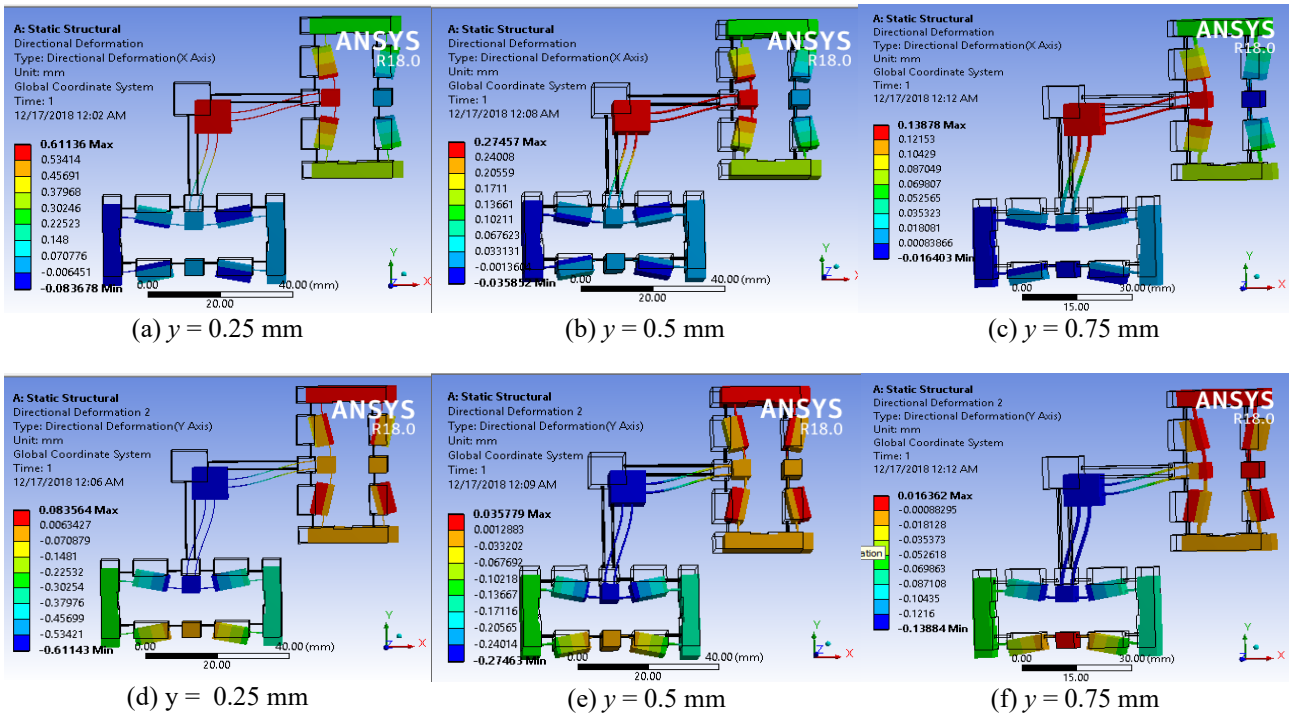
(a) y = 0.25 mm   (b) y = 0.5 mm   (c) y = 0.75 mm

(d) y = 0.25 mm   (e) y = 0.5 mm   (f) y = 0.75 mm

Figure 6. FEM outcomes of the x-direction (a), (b), (c), and y-direction (d), (e), (f) DI with variable y.

(a) y = 0.25 mm   (b) y = 0.5 mm   (c) y = 0.75 mm
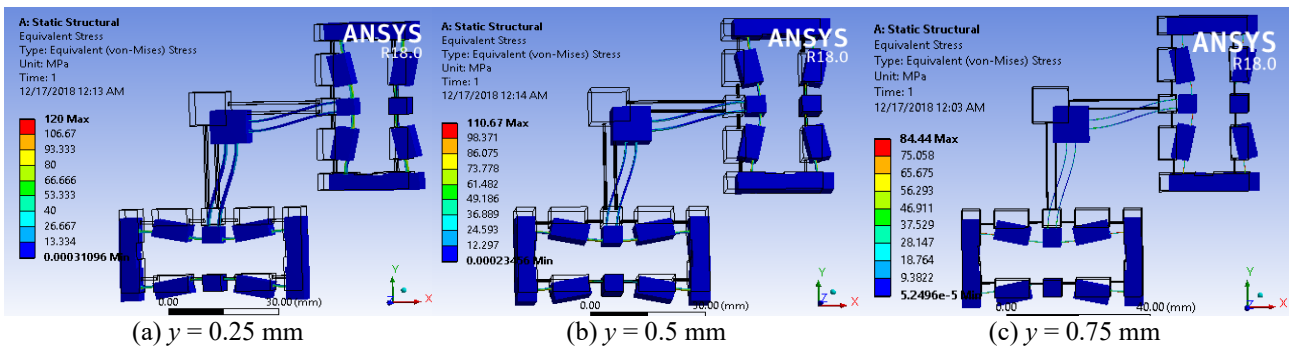
Figure 7. FEM outcomes of stress with different variable y.

(a) w = 2 mm   (b) w = 4 mm   (c) w = 6 mm

(d) w = 2 mm   (e) w = 4 mm   (f) w = 6 mm

Figure 8. FEM outcomes of the x-direction (a), (b), (c), and y-direction (d), (e), (f) DI with different variable w.

(a) w = 2 mm (b) w = 4 mm (c) w = 6 mm
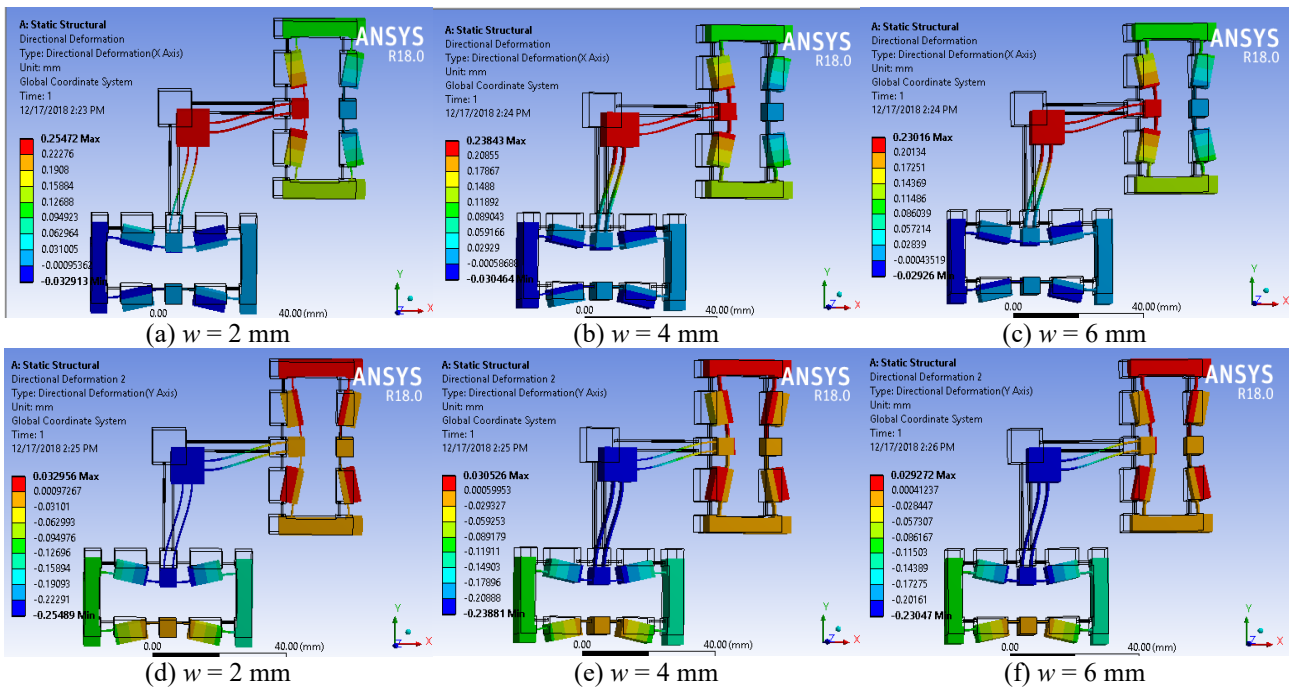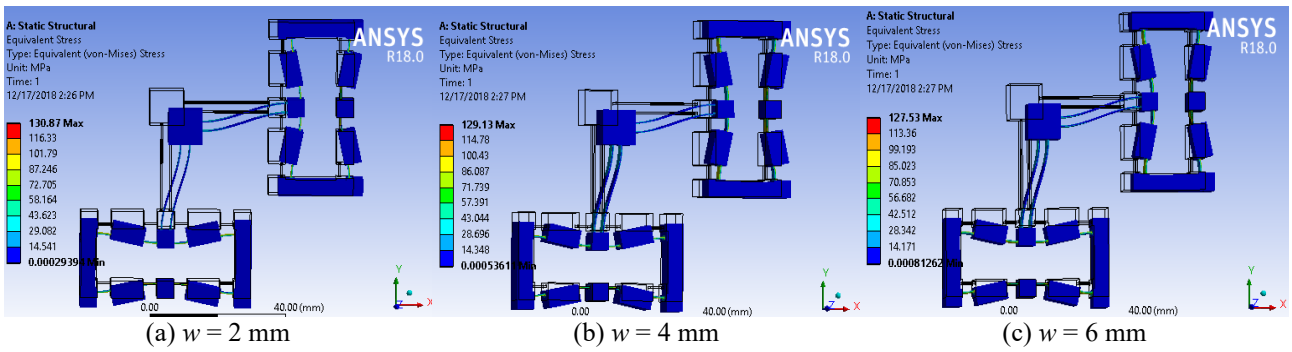
Figure 9. FEM outcomes of ST with different variable w.

Influence of Variable w

Variable w increases from 2 mm to 6 mm when x direction DI and y direction DI reduced from 0.254 mm to 0.23 mm as illustrated in Figure 8(a) and 8(b), and equivalent stress reduced from 130.87 MPa to 127.53 MPa as depicted in Figure 9. The results are better than the results presented in references [1-4, 6].

Influence of Variable x

The phenomenon indicated that variable x has been slightly influenced by DI and ST, because the direction deformation (in X-axis and Y-axis) changes from 0.643 mm to 0.682 mm, as depicted in Figure 10. The outcome of ST changes from 102.24 MPa to 109.4 MPa, as shown in Figure 11. While input DI of 0.01 mm, variable x changes from 5 mm to 15 mm, variable y of 0.25 mm, variable w of 2mm, variable t of 0 mm, and variable z of 0.8°. The magnification ratio changes from 64.3 to 68.2. These outcomes are greater than the outcomes in the references [3, 13, 15-16, 30-32].

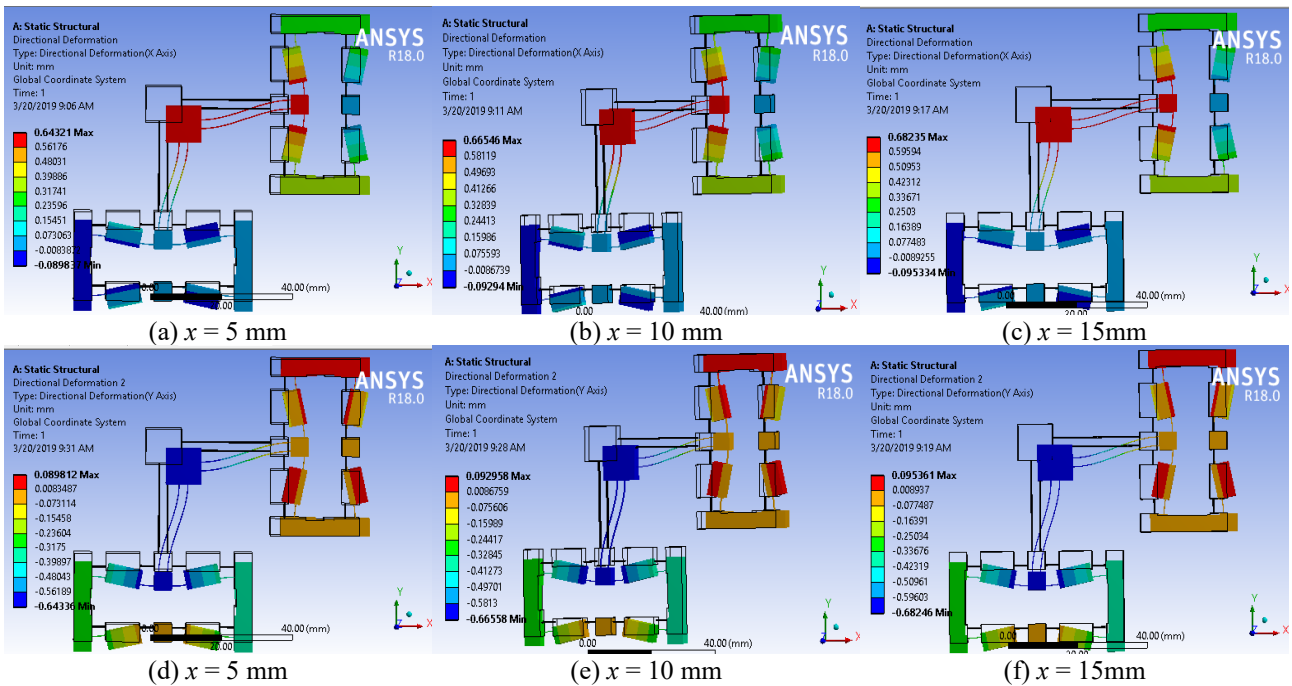(a) x = 5 mm (b) x = 10 mm (c) x = 15mm

(d) x = 5 mm (e) x = 10 mm (f) x = 15mm

Figure 10. FEM outcomes of the x-direction (a), (b), (c), and y-direction (d), (e), (f) DI with different variable x.

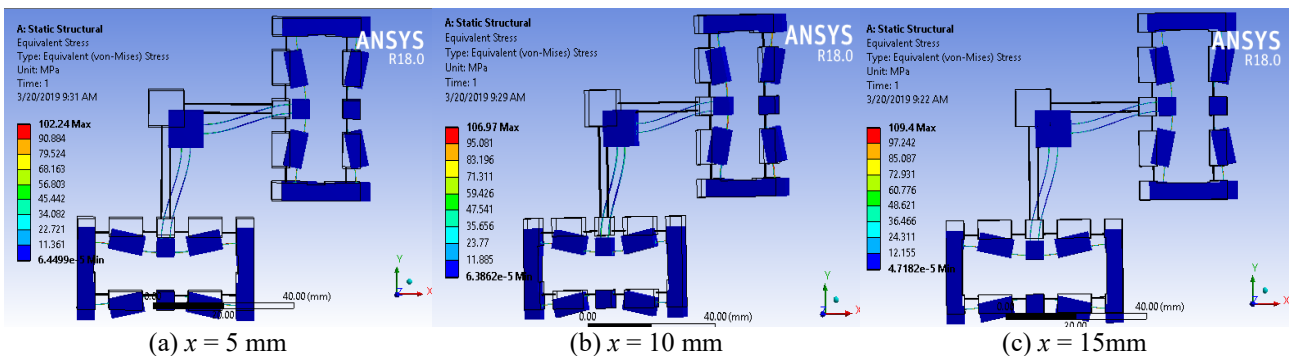(a) x = 5 mm (b) x = 10 mm (c) x = 15mm

Figure 11. FEM outcomes of ST with different variable x.

Analysis of Variance (ANOVA)

Table 4 indicated a total contribution percent of all factors to be 99.81%, with 0.19% error. It has also been identified that design dimensions have significantly been affected on the output DI among them 1.15% x, 93.02% y, 1.34% z, and 0.91% t. The F-values are larger than 2, P-values are less than 0.05, which also confirmed this result. Similarly, Table 5 also pointed out a total contribution percent is 99.81% with 0.67% error, as confirmed by the F-values and P-values.

Table 4. ANOVA for displacement.

Source	DF	Seq SS	Contribution	Adj SS	Adj MS	F-Value	P-Value
x	2	0.01360	1.15%	0.01360	0.006801	47.68	0.000
y	2	1.09581	93.02%	1.09581	0.547905	3841.66	0.000
z	2	0.01581	1.34%	0.01581	0.007905	55.42	0.000
t	2	0.01070	0.91%	0.01070	0.005351	37.52	0.000
w	2	0.03982	3.38%	0.03982	0.019909	139.59	0.000
Error	16	0.00228	0.19%	0.00228	0.000143		
Total	26	1.17802	100.00%				

R-square = 99.81%, R-square(adj) = 99.69, R-square(pred) = 99.45%

Table 5. ANOVA for stress.

Source	DF	Seq SS	Contribution	Adj SS	Adj MS	F-Value	P-Value
x	2	559.07	25.53%	559.07	279.534	76.76	0.001
y	2	132.07	6.03%	132.07	66.033	18.13	0.010
z	2	193.30	8.83%	193.30	96.650	26.54	0.005
t	2	73.03	3.34%	73.03	36.516	10.03	0.028
w	2	403.23	18.42%	403.23	201.616	55.36	0.001
x*y	4	517.12	23.62%	517.12	129.280	35.50	0.002
x*z	4	201.12	9.18%	201.12	50.279	13.81	0.013
x*w	4	96.16	4.39%	96.16	24.041	6.60	0.047
Error	4	14.57	0.67%	14.57	3.642		
Total	26	2189.66	100.00%				

R-square = 99.33%, R-square(adj) = 95.68, R-square(pred) = 69.69%

Regression Analysis

The regression equations (RE) for DI and ST were obtained by using Minitab 18 and presented in Eq. (23) and (24). The RE results were compared with simulation results and as presented in Figure 12(a) and 12(b) for DI and stress graph, respectively. The graphs identified that the simulation values and predicted values are close to one another, in which case the RE of stress have an error larger than the RE of DI.
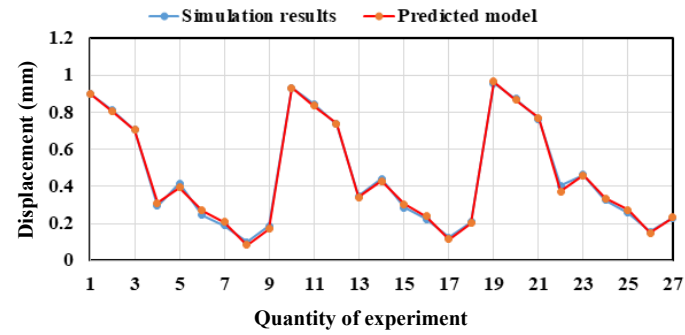
Regression equation of DI:

$$DI = 1.6982 + 0.006412x - 3.753y - 0.2272z + 0.02285t - 0.03058w + 2.452y^2 \qquad (23)$$
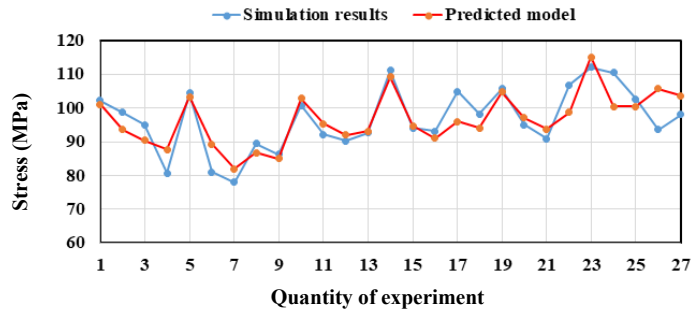
Regression equation for stress:

$$Stress = (12.11 - 0.0214x + 1.13y + 2.51z - 2.61t - 0.522w - 3.01y^2 - 6.91z^2 + 1.071t^2$$
$$+ 0.0523w^2 + 0.1568xy)^2 \qquad (24)$$

Grey Relational Analysis

Equation (1) and (2) were applied for output DI and output ST. The deviation value was determined through Eq. (3). The minimum and maximum value of the deviation value was calculated by Eq. (4) and Eq. (5). The GRC value obtained by Eq. (6). The GRG value was achieved by Eq. (14) and the values are presented in Table 6. The weight of the two output characteristics was determined by Eq. (13).

(a) DI

(b) ST

Figure 12. Comparison of simulation and the predicted values for the regression equation.

Table 6. The greater and the lesser are the better for displacement and stress, GRC, GRG and rank of GRG.

No.	$D_i^*(1)$	$D_i^*(2)$	$\Delta_{oi}(1)$	$\Delta_{oi}(2)$	$\gamma_i(1)$	$\gamma_i(2)$	ψ_i	Rank
1	0.9364	0.2893	0.0636	0.7107	0.8872	0.413	0.6509	6
2	0.8292	0.3904	0.1708	0.6096	0.7454	0.4506	0.5985	11
3	0.7058	0.5001	0.2942	0.4999	0.6296	0.5001	0.5651	12
4	0.226	0.9174	0.774	0.0826	0.3925	0.8582	0.6246	8
5	0.3681	0.2245	0.6319	0.7755	0.4417	0.392	0.4169	19
6	0.1706	0.9119	0.8294	0.0881	0.3761	0.8502	0.6123	10
7	0.1036	1	0.8964	0	0.3581	1	0.678	3
8	0	0.6604	1	0.3396	0.3333	0.5955	0.464	15
9	0.1009	0.7545	0.8991	0.2455	0.3574	0.6707	0.5135	13
10	0.9726	0.3324	0.0274	0.6676	0.948	0.4282	0.689	2
11	0.8713	0.5816	0.1287	0.4184	0.7953	0.5444	0.6703	4
12	0.745	0.6409	0.255	0.3591	0.6623	0.582	0.6223	9
13	0.2908	0.5691	0.7092	0.4309	0.4135	0.5371	0.4751	14
14	0.398	0.029	0.602	0.971	0.4537	0.3399	0.397	24
15	0.2174	0.5292	0.7826	0.4708	0.3898	0.515	0.4522	16
16	0.1434	0.5532	0.8566	0.4468	0.3686	0.5281	0.4481	17
17	0.0294	0.2081	0.9706	0.7919	0.34	0.387	0.3634	27
18	0.1269	0.4079	0.8731	0.5921	0.3641	0.4578	0.4108	21
19	1	0.1867	0	0.8133	1	0.3807	0.6914	1
20	0.9038	0.4976	0.0962	0.5024	0.8386	0.4988	0.6693	5
21	0.7752	0.6193	0.2248	0.3807	0.6898	0.5677	0.629	7
22	0.3542	0.1556	0.6458	0.8444	0.4364	0.3719	0.4043	22
23	0.422	0	0.578	1	0.4638	0.3333	0.3988	23
24	0.2622	0.0478	0.7378	0.9522	0.4039	0.3443	0.3742	26
25	0.1829	0.2761	0.8171	0.7239	0.3796	0.4085	0.394	25
26	0.0635	0.5393	0.9365	0.4607	0.3481	0.5205	0.434	18
27	0.1507	0.4124	0.8493	0.5876	0.3706	0.4597	0.415	20

The graph of the GRG value was drawn out in Figure 13. The graph of the GRG mean values of the two output characteristics, as presented in Figure 14 indicated the high peak of the variable reached the optimum level. Therefore, the combination variables at the optimum level are x3y1z1t1w1.

Table 7. ANOVA for GRG.

Source	DF	Seq SS	Contribution	Adj SS	Adj MS	F-Value	P-Value
x	2	0.012299	8.44%	0.012299	0.006150	66.65	0.001
y	2	0.083181	57.05%	0.083181	0.041590	450.78	0.000
z	2	0.009508	6.52%	0.009508	0.004754	51.53	0.001
t	2	0.000843	0.58%	0.000843	0.000422	4.57	0.093
w	2	0.004021	2.76%	0.004021	0.002010	21.79	0.007
x*y	4	0.021285	14.60%	0.021285	0.005321	57.67	0.001
x*z	4	0.009705	6.66%	0.009705	0.002426	26.30	0.004
x*w	4	0.004595	3.15%	0.004595	0.001149	12.45	0.016
Error	4	0.000369	0.25%	0.000369	0.000092		
Total	26	0.145807	100.00%				

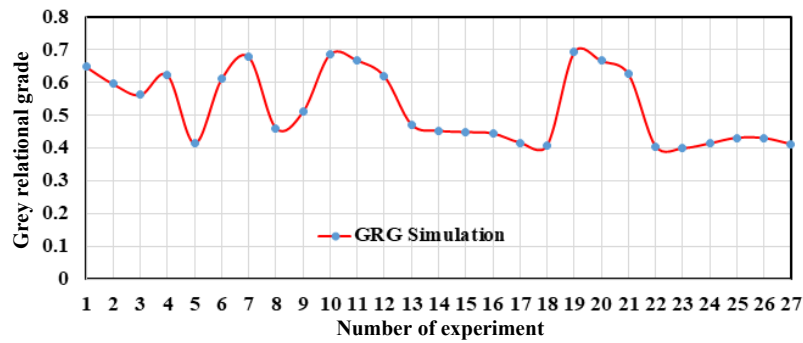R-sqaure = 99.75%, R-square(adj), R-square(pred)=88.47%

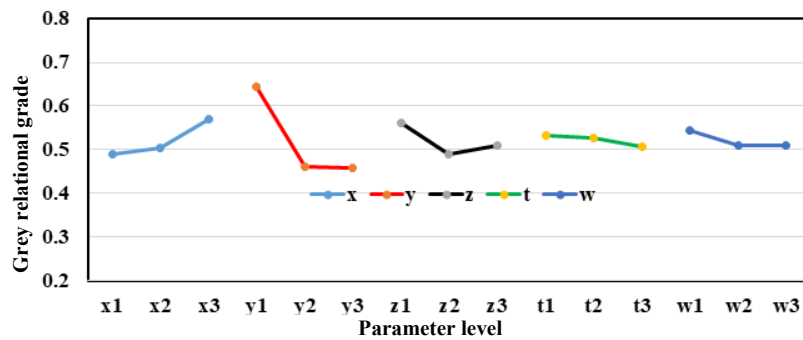
Figure 13. Plot for GRG.

Figure 14. Response graph of GRG.

Regression Equation for GRG

The RE for GRG was achieved by Minitab 18 and written in Eq. (25) and the graph was drawn in Figure 15. It is identified that the values of GRG are closed to the straight line with deviation error in the interval (-0.05,0.05).
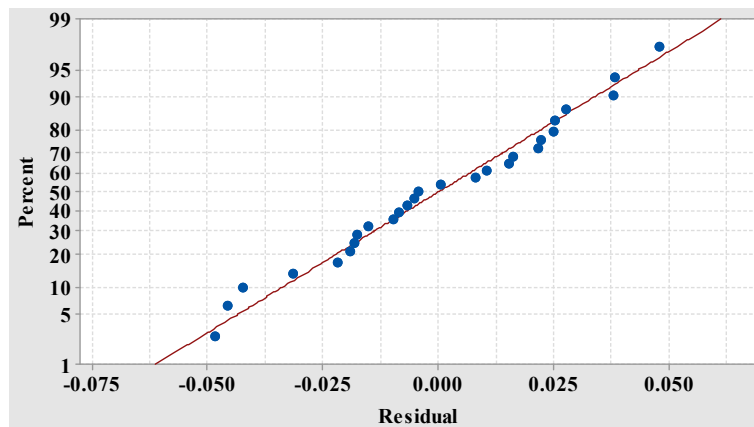

Figure 15. Residual plot for GRG.

The Outcomes of Artificial Neural Network Analysis

The training results are illustrated in Figure 15 to Figure 17, so that the performance plots indicated that the best validation performance is 1.27×10^{-7}, at epoch 0. The gradient, mu and validation checks are equal to 0.000108, 10^{-6}, 6 at epoch 6, respectively. The graphs, as pointed out in Figure 16, compared the simulation results and the predicted values of ANN for GRG. The graphs lie near to the straight line. The training, validation, test and remainder are all are equal to 0.9993, 1, 1 1nd 0.9994, respectively. The training and simulation result and error are listed in Table 8.
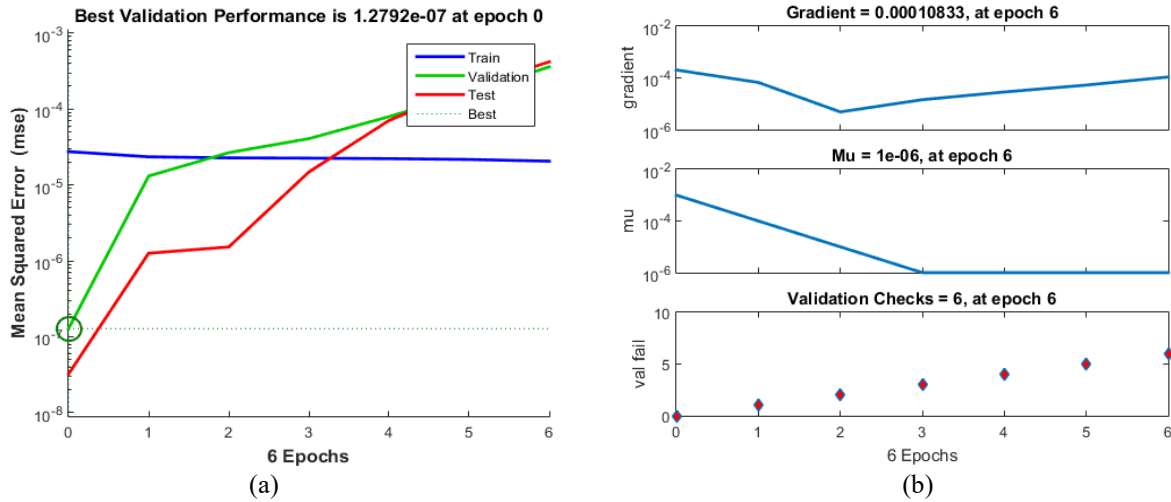

Figure 16. The results of ANN: (a) performance plot, and (b) training state of ANN for GRG.

The testing and simulation result and error are listed in Table 9. The graph compared the training, therefore testing with simulation results as demonstrated in Figure 18(a) and 18(b). The graphs lie very close to each other. The statistical analysis results, as presented in Table 10, pointed out that RE and ANN was acceptable to optimise the design compliant mechanism. Because R^2 is larger than 94%, MSE is less than 0.0007, RMSE is less than 0.03 and MAPE is less than 5%.
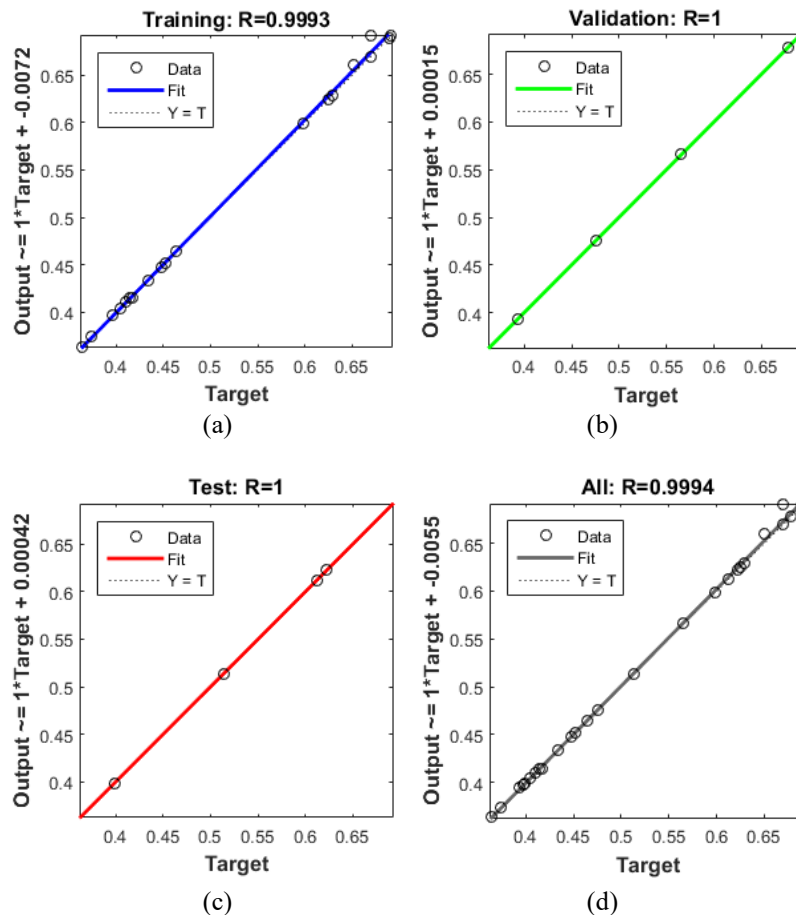

Figure 17. Relationship between simulation values and ANN of GRG.

Table 8. Design variable, simulation outcomes, training results and error of GRG.

Trial No.	x	y	z	t	w	GRG simulation	GRG predicted
1	5	0.25	0	0.8	2	0.6509	0.6601
2	5	0.25	0.2	1.2	4	0.5985	0.5984
3	5	0.25	0.4	1.6	6	0.5651	0.5699
4	5	0.5	0	1.2	6	0.6246	0.6246
5	5	0.5	0.2	1.6	2	0.4169	0.4147
6	5	0.5	0.4	0.8	4	0.6123	0.6120
7	5	0.75	0	1.6	4	0.678	0.6779
8	5	0.75	0.2	0.8	6	0.464	0.4640
9	5	0.75	0.4	1.2	2	0.5135	0.5137
10	10	0.25	0	0.8	2	0.689	0.6895
11	10	0.25	0.2	1.2	4	0.6703	0.6911
12	10	0.25	0.4	1.6	6	0.6223	0.6223
13	10	0.5	0	1.2	6	0.4751	0.4751
14	10	0.5	0.2	1.6	2	0.3970	0.3970
15	10	0.5	0.4	0.8	4	0.4522	0.4522
16	10	0.75	0	1.6	4	0.4481	0.4481
17	10	0.75	0.2	0.8	6	0.3634	0.3635
18	10	0.75	0.4	1.2	2	0.4108	0.4108
19	15	0.25	0	0.8	2	0.6914	0.6914
20	15	0.25	0.2	1.2	4	0.6693	0.6692
21	15	0.25	0.4	1.6	6	0.629	0.6291
22	15	0.5	0	1.2	6	0.4043	0.4042
23	15	0.5	0.2	1.6	2	0.3988	0.3987
4	15	0.5	0.4	0.8	4	0.3742	0.3741
25	15	0.75	0	1.6	4	0.394	0.3941
26	15	0.75	0.2	0.8	6	0.434	0.4340
27	15	0.75	0.4	1.2	2	0.415	0.4150

Table 9. Design variables, simulation, testing outcomes GRG.

Trial No.	x	y	z	t	w	GRG Simulation	GRG Predicted
1	5	0.25	0	0.8	2	0.6509	0.66014
2	5	0.25	0.2	1.2	4	0.5985	0.59849
3	5	0.25	0.4	1.6	6	0.5651	0.56579
4	10	0.5	0	1.2	6	0.4751	0.4751
5	10	0.5	0.2	1.6	2	0.397	0.397
6	10	0.5	0.4	0.8	4	0.4522	0.4522
7	15	0.75	0	1.6	4	0.394	0.3941
8	15	0.75	0.2	0.8	6	0.434	0.434
9	15	0.75	0.4	1.2	2	0.415	0.415

Table 10. Statistical analysis results for predicted models.

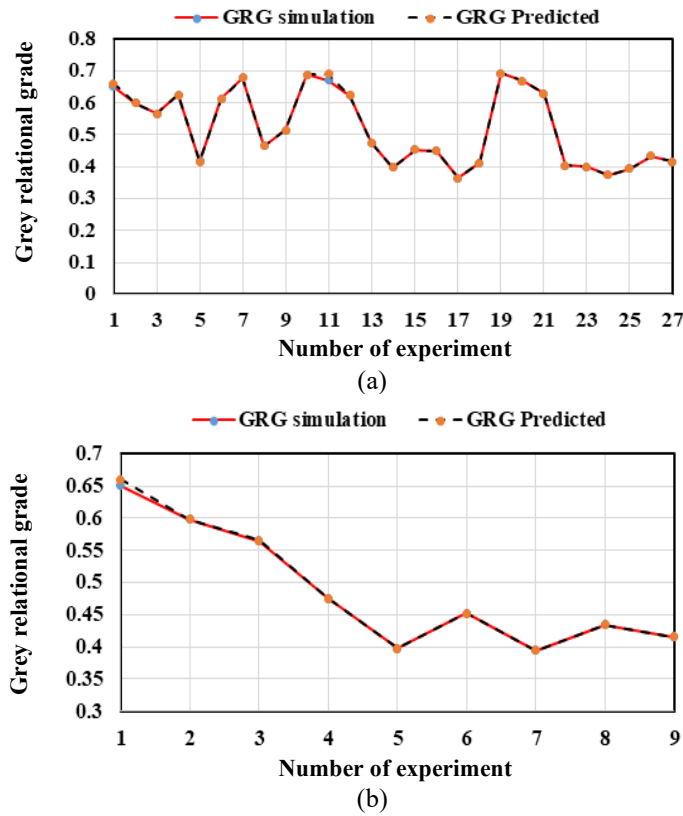| Criteria	Predicted models			
	Regression equation of GRG		ANN of GRG	
	Training	Testing	Training	Testing
R^2 (%)	94.91	99.62	99.85	99.88
MSE	0.000671	0.00025	0.000019	0.00001
RMSE	0.025907	0.01602	0.0044	0.00178
MAPE (%)	4.48	1.67	0.2	0.06

(a)

(b)

Figure 18. The (a) training and (b) testing graph of GRG simulation compare with GRG predicted ANN.

The Outcome of Predicted Optimisation

The optimum values of the DI, the ST, and GRG gained 0.95698 mm, 105.74 MPa, and 0.6914, respectively. The predicted values for the output DI and the output ST and the GRG obtained by Eq. (15) to (17) and values, as depicted in Table 11 are 0.9625 mm, 108.0036 MPa, and 0.7661, respectively. The results are in agreement with the deviation of DI, ST, and GRG; and, they are 0.57%, 2.1% and 9.75%, respectively, as written in Table 11 and Table 12.

Table 11. Response table of average of DI, ST and GRG.

Response	Level	x	y	z	t	w
	1	0.4281	0.8370	0.5013	0.4482	0.5266
	2	0.4618	0.3586	0.4704	0.4674	0.4513
DI	3	0.4922	0.1866	0.4104	0.4665	0.4043
	Delta	0.0641	0.6505	0.0909	0.0192	0.1223
	Rank	4	1	3	5	2
	1	90.700	96.690	94.890	95.730	100.450
	2	94.950	96.500	97.570	94.230	92.070
ST	3	99.520	91.980	92.710	95.210	92.650
	Delta	8.820	4.710	4.860	1.500	8.380
	Rank	1	4	3	5	2
	1	0.490	0.643	0.562	0.531	0.544
	2	0.503	0.461	0.490	0.526	0.509
GRG	3	0.569	0.458	0.511	0.505	0.509
	Delta	0.079	0.185	0.072	0.026	0.035
	Rank	2	1	3	5	4

First, the average values of the displacement and stress were presented in Tables 4 and 5, respectively. Second, μ_D and μ_σ were achieved by Eq. (15), Eq. (16) and are shown in Table 6 and Table 7. The total average values of displacement and stress are equal to 0.4607 mm and 96.6491 MPa, μ_D and μ_σ were determined, as follows:

$$\mu_D = D_m + \sum_{i=1}^{q}(D_0 - D_M) = x3 + y1 + z1 + t1 + w1 = 0.49922 + 0.837 + 05013 + 04482 + 0.566 - 4*0.4607$$
$$= 0.9625\,(\text{mm})$$

$$\sigma_D = s_m + \sum_{i=1}^{q}(\sigma_0 - \sigma_M) = x3 + y1 + z1 + t1 + w1 = 101.74 + 96.8 + 95.89 + 98.06 + 102.11 - 4*96.6491$$
$$= 108.0036 \,)\,(MPa)$$

At 95% confidence interval to confirm *(CI)* was gained utilising Eq. (18), Table 4, Table 5 and Table 7.

i.   For DI, at α=0.05, fe =16, $F_{0.05}(1,16)$ = 4.494 [30], Ve =0.001265, R = 10, Re = 1, n = 27.

$$CI_{CE} = \pm\sqrt{4.494 \times 0.000143 \times \left(\frac{1}{\frac{27}{1+10}} + 1\right)} = \pm 0.03 \quad 0.9325 < \mu_{confirmation} < 0.9925$$

ii.   For ST, at α=0.05, fe =4, $F_{0.05}(1,4)$ = 7.7086 [30], Ve =3.642, R = 22, Re = 1, n = 27

$$CI_{CE} = \pm\sqrt{7.7086 \times 3.642 \times \left(\frac{1}{\frac{27}{1+22}} + 1\right)} = \pm 7.21 \quad 100.7936 < \mu_{confirmation} < 115.2136$$

iii.   For GRG, at α=0.05, fe =4, $F_{0.05}(1,4)$ = 7.7086 [30], Ve =0.000092, R = 22, Re = 1, n = 27

$$CI_{CE} = \pm\sqrt{7.7086 \times 0.000092 \times \left(\frac{1}{\frac{27}{1+22}} + 1\right)} = \pm 0.03624 \quad 0.72986 < \mu_{confirmation} < 0.80234$$

The compared results predicted values with optimal GRG values of the methods, as shown in Table 12. Results identified that the methods are in agreement with a deviation error of 9.75% for GRA, 6.47% for RE, and 6.22% for ANN. The compared results between the predicted and optimal DI values of methods demonstrated that the method is in agreement with a deviation of 6.86% for the Taguchi method, 0.0034% for RE, 0.57% for GRA, and 0.52% for ANN. The compared results between the predicted and optimal ST values of methods demonstrated that the method is in agreement with a deviation of 8.41% for the Taguchi method, 3.67% for RE, and 2.1% for both GRA and ANN.

Table 12. Comparison of the predicted and optimal GRG and DI values.

| Response		Optimal combination	GRA	Regression	ANN
GRG	Predicted		0.7661	0.6292	0.6484
	Optimal	x3y1z1t1w1	0.6914	0.6727	0.6914
	Error (%)		9.75	6.47	6.22
DI	Predicted		0.9625	0.984813	0.9625
	Optimal	x3y1z1t1w1	0.95698	0.98478	0.96245
	Error (%)		0.57	0.0034	0.52
ST	Predicted		108.0036	108.0615	108.0036
	Optimal	x3y1z1t1w1	105.74	104.0876	105.74
	Error (%)		2.1	3.67	2.1

The optimum model obtained by using the regression equation, GRA and ANN is x3y1z1t1w1 which was utilised to analyse DI and ST in a static structure in ANSYS. The outcomes indicated that DI and ST were approximated using the optimal results. The outcomes are also compared with the kind of finite element tetrahedron and hexagon, as depicted in Figure 19.
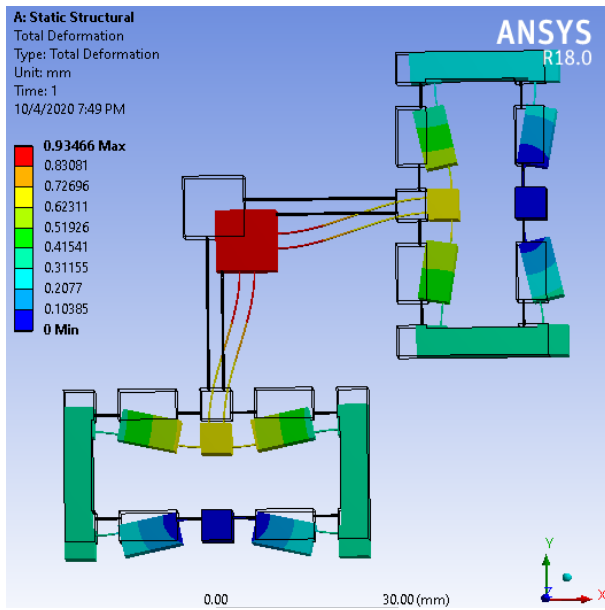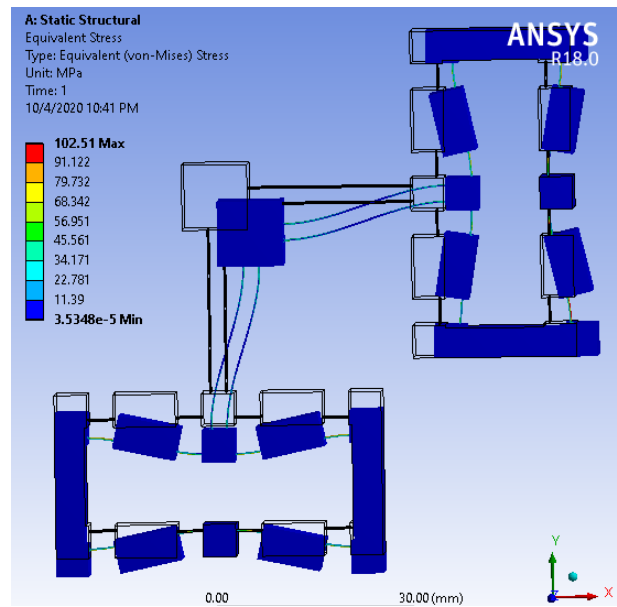
(a) The outcome of DI - mesh divided with tetrahedron elements
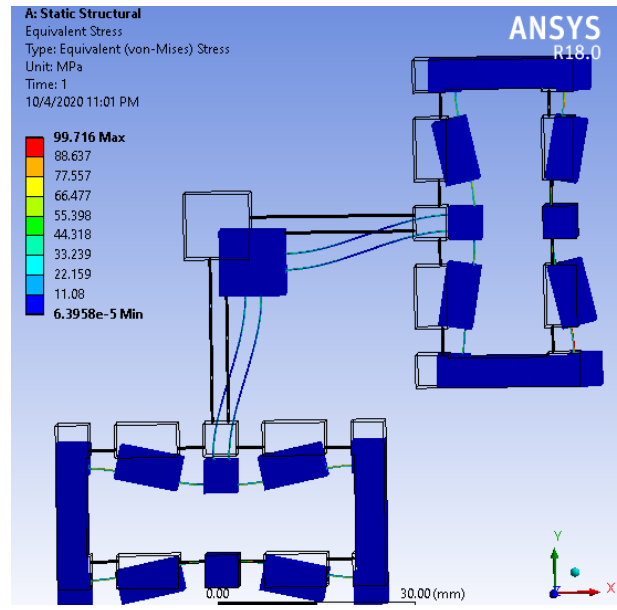
(b) The outcome of ST - mesh divided with tetrahedron elements
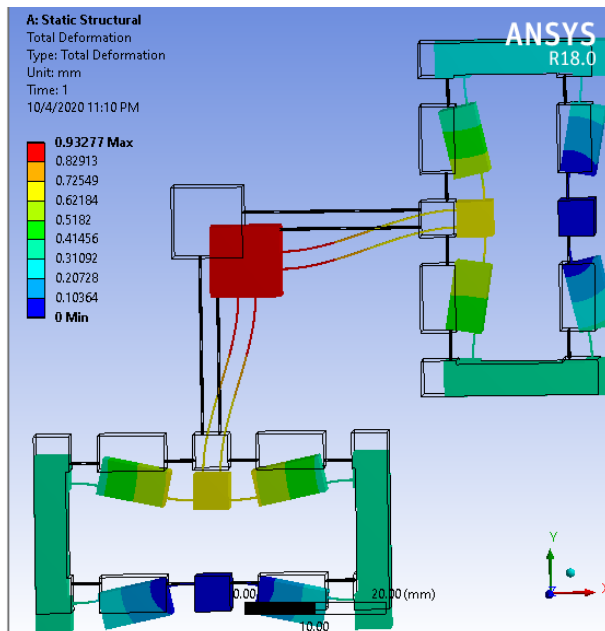
(c) The outcome of DI - mesh divided with hexagon element

(d) The outcome of ST - mesh divided with hexagon elements

Figure 19. The optimal results with different kinds of finite element.

CONCLUSION

The investigation proved the influence of design variables on the magnification ratio of 2-DOF BTCMFH by ANSYS. The FEM outcomes indicated variable y significantly influenced the magnification and stress, and the remaining variables have slightly influenced. The outcomes proved the studied mechanism has more advantage than the previous publication. It indicated that the studying mechanism has a magnification ratio greater than what is found in some previous publications. Moreover, the FEM outcomes are all confirmed by means of ANOVA, regression analysis, surface plot, GRA and ANN. The optimum outcomes proved that the design variables have a significant effect on magnification ratio and stress. In rank order, the first is variable y, second is variable w, third is variable z, fourth is variable x, and the final is variable t. The optimum values of displacement and the stress obtained are 0.9570 mm and 105.74 MPa, respectively. The amplification ratio x- and y-axis direction achieved 67.7 times. The forecasted values of DI and ST achieved 0.9625 mm and 108.0036 MPa, respectively. The amplification of both the x- and y-axis direction ratio achieved 68.06, with the outcomes, error between forecasted, and optimum values of displacement and stress being 0.57% and 2.1%, respectively.

ACKNOWLEDGEMENT

REFERENCES

[1]   Yong YK, Lu TF. Kinetostatic modeling of 3-RRR compliant micro-motion stages with flexure hinges. Mechanism and Machine Theory, 2009. 44(6): 1156-1175.

[2]   Tian Y, Shirinzadeh B, Zhang D. Design and dynamics of a 3-DOF flexure-based parallel mechanism for micro/nano manipulation. Microelectronic Engineering, 2010. 87(2): 230-241.

[3]   Qi KQ, Xiang Y, Fang C, Zhang Y, Yu CS. Analysis of the displacement amplification ratio of bridge-type mechanism. Mechanism and Machine Theory, 2015. 87: 45-56.

[4]   Qiu L, Yin S, Xie Z, Failure analysis and performance comparison of Triple-LET and LET flexure hinges. Engineering Failure Analysis, 2016. 66: 35-43.

[5]   Tian Y, Shirinzadeh B, Zhang D. Closed-form compliance equations of filleted V-shaped flexure hinges for compliant mechanism design. Precision Engineering, 2010. 34(3): 408-418.

[6]   Yang M, Du Z, Dong W. Modeling and analysis of planar symmetric super-elastic flexure hinges. Precision Engineering, 2016. 46: 177-183.

[7]   Dao TP. Multiresponse Optimization of a Compliant Guiding Mechanism Using Hybrid Taguchi-Grey Based Fuzzy Logic Approach. Mathematical Problems in Engineering, 2016. 2016: 1-17.

[8]   Dao TP, Huang SC. Robust design for a flexible bearing with 1-DOF translation using the Taguchi method and the utility concept. Journal of Mechanical Science and Technology, 2015. 29(8): 3309-3320.

[9]   Dao TP, Huang SC. Design and analysis of a compliant micro-positioning platform with embedded strain gauges and viscoelastic damper. Microsystem Technologies, 2016. 23(2): 441-456.

[10]   Dao TP, Huang SC. Optimisation of a two degrees of freedom compliant mechanism using Taguchi method-based grey relational analysis. Microsystem Technologies, 2017. 23(10): 4815-4830.

[11]   Dao TP, Huang SC. Design and multi-objective optimisation for a broad self-amplified 2-DOF monolithic mechanism. Sādhanā, 2017. 42(9): 1527-1542.

[12]   Dao TP, Huang SC. Compliant thin-walled joint based on zygoptera nonlinear geometry. Journal of Mechanical Science and Technology, 2017. 31(3): 1293-1303.

[13]   Xu Q, Li Y. Analytical modeling, optimisation and testing of a compound bridge-type compliant displacement amplifier. Mechanism and Machine Theory, 2011. 46(2): 183-200.

[14]   Liu P, Yan P. A new model analysis approach for bridge-type amplifiers supporting nano-stage design. Mechanism and Machine Theory, 2016. 99: 176-188.

[15]   Ling M, Cao J, Zeng M, Lin J, Inman DJ. Enhanced mathematical modeling of the displacement amplification ratio for piezoelectric compliant mechanisms. Smart Materials and Structures, 2016. 25(7): 075022.

[16]   Choi KB, Lee JJ, Kim GH, Lim HJ, Kwon SG. Amplification ratio analysis of a bridge-type mechanical amplification mechanism based on a fully compliant model. Mechanism and Machine Theory, 2018. 121: 355-372.

[17]   Ma HW, Yao SM, Wang LQ, Zhong Z. Analysis of the displacement amplification ratio of bridge-type flexure hinge. Sensors and Actuators A: Physical, 2006. 132(2): 730-736.

[18]   Ling M, Cao J, Jiang Z, Lin J. Modular kinematics and statics modeling for precision positioning stage. Mechanism and Machine Theory, 2017. 107: 274-282.

[19]   Ling M, Cao J, Jiang Z, Lin J. A semi-analytical modeling method for the static and dynamic analysis of complex compliant mechanism. Precision Engineering, 2018. 52: 64-72.

[20]   Sabri MFM, Ono T, Esashi M. Modeling and experimental validation of the performance of a silicon XY-microstage driven by PZT actuators. Journal of Micromechanics and Microengineering, 2009. 19(9): 095004.

[21]   Šalinić S, Nikolić A. A new pseudo-rigid-body model approach for modeling the quasi-static response of planar flexure-hinge mechanisms. Mechanism and Machine Theory, 2018. 124: 150-161.

[22]   Lai LJ, Zhu ZN. Design, modeling and testing of a novel flexure-based displacement amplification mechanism. Sensors and Actuators A: Physical, 2017. 266: 122-129.

[23]   Wang R, Zhang ZN. A planar 3-DOF nano-positioning platform with large magnification. Precision Engineering, 2016. 46: 221-231.

[24]   Kumar S, Meenu, Investigation of surface roughness and material removal rate for UD-GFRP composite using Taguchi grey relational analysis. International Journal of Automotive and Mechanical Engineering, 2017. 14(2): 4298-4314.

[25]   Panda A, Sahoo AK, Panigrahi I, Rout AK. Investigating Machinability in Hard Turning of AISI 52100 Bearing Steel Through Performance Measurement: QR, ANN and GRA Study. International Journal of Automotive and Mechanical Engineering, 2018. 15(1): 4935-4961.

[26]   Abu MY, Jamaluddin KR, Zakaria MA. Classification of crankshaft remanufacturing using Mahalanobis-Taguchi system. International Journal of Automotive and Mechanical Engineering, 2016. 13(2): 3413-3422.

[27]   Rao VR, Ramanaiah N, Rao MS, Sarcar MMM, Kartheek G. Optimisation of process parameters for minimum volumetric wear rate on AA7075-TiC metal matrix composite. International Journal of Automotive and Mechanical Engineering, 2016. 13(3): 3669-3680.

[28]   Huynh NT, Huang SC, Dao TP, Optimal displacement amplification ratio of bridge-type compliant mechanism flexure hinge using the Taguchi method with grey relational analysis. Microsystem Technologies, 2018: 1-15.

[29]   Huynh NT, Huang SC, Dao TP, Design variables optimisation effects on acceleration and contact force of the double sliders-crank mechanism having multiple revolute clearance joints by use of the Taguchi method based on a grey relational analysis. Sādhanā, 2020. 45(1).

[30]   Roy RK. A primer on the Taguchi method, 2nd sed. Society of Manufacturing Engineers; 2010.

[31]   Kumar S, Batish A, Singh R, Singh TP. A hybrid Taguchi-artificial neural network approach to predict surface roughness during electric discharge machining of titanium alloys. Journal of Mechanical Science and Technology, 2014. 28(7): 2831-2844.

[32]   Kant G, KS Sangwan. Predictive modelling and optimisation of machining parameters to minimise surface roughness using artificial neural network coupled with genetic algorithm. Procedia CIRP, 2015. 31: 453-458.

[33]   Sukumar MS, Ramaiah PV, Nagarjuna A. Optimization and prediction of parameters in face milling of Al-6061 using Taguchi and ANN approach. Procedia Engineering, 2014. 97: 365-371.

[34]   Dao TP, Huang SC. Design, fabrication, and predictive model of a 1-Dof translational flexible bearing for high precision mechanism. Transactions of the Canadian Society for Mechanical Engineering 2015. 39(3): 419-429.